Support effects in the hydrogenation of cinnamaldehyde over carbon nanofiber-supported platinum catalysts: characterization and catalysis

Marjolein L. Toebes [a], Yihua Zhang [a], Jan Hájek [b], T. Alexander Nijhuis [a], Johannes H. Bitter [a], A. Jos van Dillen [a], Dmitry Yu. Murzin [b], Diek C. Koningsberger [a], Krijn P. de Jong [a,*]

[a] *Department of Inorganic Chemistry and Catalysis, Debye Institute, Utrecht University, P.O. Box 80 083, 3508 TB Utrecht, Netherlands*
[b] *Laboratory of Industrial Chemistry, Process Chemistry Group, Åbo Akademi University, Turku/Åbo, Finland*

Abstract

Carbon nanofiber-supported platinum catalysts were studied to establish the influence of the support surface composition on their performance in the liquid-phase hydrogenation of cinnamaldehyde. By acid–base titration, XPS, and TGA-MS, the number of oxygen-containing surface groups was determined in oxidized carbon nanofiber samples and in platinum catalysts pretreated at 473–973 K. TEM, EXAFS, and H_2-chemisorption studies showed the presence of a narrow and stable platinum particle-size distribution (1–2 nm). The overall catalytic activity increased by a factor of 25 after treatment at 973 K, which is tentatively related to the decreasing amount of oxygen of the carbon fibers. With XPS and H_2-chemisorption experiments carried out at 308 K no clear evidence was found for a change in the electronic structure of the platinum particles induced by the oxygen-containing groups present on/in the surface of the carbon nanofibers. A linear decrease of the hydrogenation activity with an increase of the number of acidic groups on the carbon nanofiber support was found. Therefore, it is suggested that hydrogenation is assisted by adsorption of cinnamaldehyde on the carbon support after removal of the oxygen-containing surface groups.
© 2004 Elsevier Inc. All rights reserved.

Keywords: Carbon nanofibers; CNF; Platinum catalyst; Oxygen-containing surface groups; Cinnamaldehyde hydrogenation; Metal–support interaction

1. Introduction

The selective hydrogenation of α, β-unsaturated aldehydes to unsaturated alcohols is a key step especially in the preparation of various fine chemicals [1–4]. In the literature often noble metals supported on titania and graphitic carbon are used either with or without a promoter, to obtain a high alcohol selectivity [1,3,5–9]. Recently several publications have appeared in which carbon nanofibers (CNF) or multi-walled carbon nanotubes (MWNT) are examined as catalyst support [10]. For this type of reactions promising results were found. For example, in the liquid-phase hydrogenation of cinnamaldehyde with MWNT-supported ruthenium catalysts [7,11,12] selectivities to cinnamyl alcohol up to 92% have been observed, whereas alumina-supported ruthe-

nium catalysts gave rise to selectivities of 20–30% [6]. With activated carbon-supported ruthenium catalysts selectivities upto 30–40% have been obtained [13]. Often the increased selectivity toward the unsaturated alcohol is explained in terms of transfer of π-electrons from the graphitic planes to the metal particles [7,11,14]. In this way the charge density on the metal increases, enhancing π_{CO}^* backbonding and thus increasing the probability for the C=O bond hydrogenation.

Earlier we reported on the influence of oxygen-containing surface groups in the liquid-phase hydrogenation of cinnamaldehyde using CNF-supported ruthenium catalysts [15]. In that study we used well-defined Ru/CNF catalysts with highly dispersed and uniform ruthenium particles of 1–2 nm. A clear trend was observed in activity and selectivity with the number of oxygen-containing surface groups. The rate of cinnamaldehyde conversion was enhanced by a factor of 22 after removal of the major-

---

ity of the surface oxygenates which was mainly due to a strong increase in the hydrogenation rate of the C=C bond.

A possible explanation for a direct effect of the oxygen-containing surface groups can be found in the adsorption of the organic reactant [16–18]. After increasing treatment temperatures, the CNF surface gradually changes from polar to nonpolar due to the removal of the oxygen-containing surface groups. This change in polarity might change the preferential adsorption mode of cinnamaldehyde and enable adsorption of the reactant on the CNF support, thereby influencing the activity and selectivity. An alternative explanation implies the indirect influence of the oxygen-containing groups on catalysis via the electronic state of the metal. This model is based on the work of Koningsberger and co-workers and concerns the interaction between small (< 2 nm) metal particles and oxidic supports [19–21]. With decreasing electron richness of the support oxygen atoms, the density of states (DOS) and the Fermi level of the metal particles shift to a higher binding energy. This effect has been observed with XPS, FTIR, and XAFS. For carbon-supported noble metal catalysts this model suggests that lower amounts of (more electronegative) oxygen in the carbon support would give rise to a change in the electronic structure of the metal.

Our previous work on Ru/CNF [15] has not been conclusive whether electronic or adsorption effects are predominant in steering catalysis. A fundamental study of the electronic properties of the ruthenium particles was hampered by among others the overlap of the carbon and ruthenium peaks in XPS. For platinum more precise XPS measurements can be carried out while H_2 chemisorption can be related to earlier results. The study of metal–support interaction with oxidic supports has largely been performed with platinum catalysts [19–21].

To gain more insight in the nature of the distinct influence of oxygen-containing surface groups, here we report on the influence of these groups in CNF-supported platinum catalysts in the liquid-phase hydrogenation of cinnamaldehyde. This investigation is performed on well-defined Pt/CNF catalysts with metal particles of 1–2 nm with a narrow particle-size distribution and a tunable amount of support surface oxygen. A well-defined catalyst with small and uniform metal particles is needed to enable observation of the electronic support effect at all [22]. In this paper we discuss the characteristics of the CNF and the type and number of oxygen-containing surface groups present after activation and heat treatment in N_2. With XPS and H_2-chemisorption experiments we investigate whether the catalytic performance of the Pt/CNF system is related to an electronic effect, similar to that described for oxide-supported catalysts. The influence of the oxygen groups on the adsorption of the reactant on the CNF support is dealt with in the accompanying paper.

Table 1
Sample codes, loadings, and pretreatment conditions of the various CNF-supported platinum catalysts

Sample	Loading (wt%) XRF	Gas-phase prereduction	Heat treatment in N_2
PtCNFnp[a]	3.6	–	–
PtCNF	3.6	473 K	–
PtCNF573	3.6	473 K	573 K
PtCNF773	3.6	473 K	773 K
PtCNF973	3.6	473 K	973 K

[a] np, not prereduced in the gas-phase.

2. Experimental

2.1. Synthesis carbon nanofiber-supported platinum catalyst

Carbon nanofibers were grown from H_2/CO over a Ni/SiO_2 catalyst as described in [15].

Platinum (intake 5 wt%) was deposited on the fibers according to a HDP method. To an acidified suspension (pH 3) of 5 g CNF in 250 ml demiwater heated up to 363 K under inert atmosphere, 0.41 g urea (Acros) and 0.52 g $Pt(NH_3)_4(NO_3)_2$ (Aldrich) were added under vigorous stirring. The pH of the slurry was monitored, to follow the process and to indicate its completeness. After 18 h the loaded CNF were filtered and washed thoroughly with demiwater, dried at 353 K in an N_2 flow, and reduced in flowing H_2 at 473 K for 1 h (heating rate = 5 K/min). Next the samples were exposed to air at RT.

In order to obtain different concentrations of oxygen-containing surface groups on the CNF, samples of the freshly reduced catalyst were heat-treated in an N_2 flow for 2 h at 573, 773, and 973 K [23]. The catalyst samples together with their identification codes are listed in Table 1.

2.2. Catalyst characterization

The numbers of acid sites of the oxidized CNF after the various heat treatments were determined by standard acid–base titrations as described in [23]. The total number of thermally removable oxygen-containing groups was determined by TGA [23].

The CNF-supported platinum catalysts were examined in a Philips CM-200 FEG TEM and a Tecnai 20 FEG TEM both operated at 200 kV. After suspending in ethanol under ultrasonic vibration, samples were brought onto a holey carbon film on a copper grid.

Platinum loadings were determined by means of XRF on a Philips PW 1480. Before analysis the Pt/CNF samples were pressed into a tablet using a methyl methacrylate binder.

XPS analyses were performed on a Fisons ESCALAB 210I-XL and a Vacuum Generators XPS system as described earlier [23].

Hydrogen-chemisorption measurements were performed using a Micromeritics ASAP 2010C. Each sample was dried

in He at 393 K for 1 h, and reduced in flowing H_2 (flow rate = 50 ml/min STP) at 473 K for 2 h, heating rate 5 K/min. After reduction the samples were degassed for 2 h at 10^{-1} Pa at the reduction temperature in order to remove chemisorbed hydrogen and water. The isotherms were measured at 308 K. The presented H/Pt ratios are based on the amounts adsorbed at zero pressure found by extrapolation of the linear part of the isotherm. Calculations have been made with the total amount of adsorbed hydrogen, because XAFS results of Oudenhuijzen et al. with Pt/Al_2O_3 catalysts unambiguously show that also "weakly" bonded hydrogen is chemisorbed and must be taken into account [24]. Estimated average particle sizes and dispersions are based on spherical geometry and an adsorption stoichiometry of $H/Pt_s = 1$. The average Pt particle size, d, was calculated from

$$dD = 10^{21} \frac{6M\rho_{site}}{\rho_{metal}N},$$

where d is the average platinum particle size (nm), D is the dispersion (H/Pt), M is the atomic weight (Pt = 195.09 g/mol), ρ_{site} is the platinum surface site density (12.5 Pt atoms/nm^2), ρ_{metal} the metal density (21.45 g/cm^3), and N the Avogadro constant (6.022×10^{23} mol^{-1}) giving $d = 1.13/D$ (nm) [25].

2.3. XAFS experiments

XAFS spectra at the Pt L_3 edge were taken at the HASYLAB (Hamburg, Germany) synchrotron beamline X1.1, equipped with a Si(311) double-crystal monochromator. The monochromator was detuned to 50% of the maximum intensity to avoid higher harmonics present in the X-ray beam. The measurements were done in transmission mode using ion chambers filled with an Ar/N_2 mixture to have an μx of 20% in the first and a μx of 80% in the second ionization chamber. The energy of the X-ray beam was calibrated by using a Pt foil between the second and third ionization chamber.

The powdered catalysts were diluted with boron nitride and pressed into a self-supporting wafer (calculated to have an absorbance of 2.5) mounted in a stainless-steel in situ cell equipped with Be windows. The samples were re-reduced in situ at 473 K for 30 min (5 K/min) in flowing H_2 and cooled down in an H_2 atmosphere. The reduced samples are considered to be fully covered with hydrogen and are further denoted by (RED). Next the EXAFS data for the L_3 edge were collected ($T = 77$ K).

Extraction of the EXAFS data from the measured absorption spectra was performed with the XDAP code [26]. Three scans were averaged and the preedge was subtracted using a modified Victoreen curve. The background was subtracted employing cubic spline routines with a continuously adjustable smooth parameter. Normalization was performed by dividing the data by the edge step at 50 eV after the adsorption edge.

Data for phase shifts and backscattering amplitudes for Pt–Pt and Pt–C were obtained from FEFF7 and FEFF8 calculations, respectively, and calibrated by the experimental data of Pt foil and $[Rb_2Pt(CN)_4] \cdot 1.5H_2O$. Data analysis of the CNF-supported platinum catalysts was performed by multiple shell fitting using the difference file technique in R space ($1.6 < R < 3.2$ Å) with the XDAP code using both k^1 and k^3 weighting [27,28].

The variances of the magnitude and imaginary part of the Fourier transforms of fit and data were calculated according to

$$\text{Variance} = \frac{\int[\text{FT}^n_{model}(R) - \text{FT}^n_{exp}(R)]^2 dR}{\int[\text{FT}^n_{exp}(R)]^2 dR} \times 100$$

with $\text{FT}^n = \text{FT}[k^n\chi(k)]$. In this study the statistical significance of a contribution has been checked by a comparison of the amplitude of $(\text{Fit})_j$ with the noise level present in the difference file.

2.4. Catalytic experiments

Liquid-phase hydrogenation of cinnamaldehyde was studied in a 500-ml stirred semibatch reactor equipped with a sample port, reagent injection port, gas inlet, and vent.

The catalysts (0.2 g) were (re)-activated in suspension in i-propanol (220 ml) at 383 K with H_2 at a total pressure of 3.0 MPa (hydrogen partial pressure 2.8 MPa) for 30 min in the stirred autoclave (1500 rpm) prior to the introduction of cinnamaldehyde (3.0 g). All reactions were executed at 383 K using a total pressure of 5.0 MPa (hydrogen partial pressure 4.8 MPa). Samples were withdrawn periodically and analyzed on a gas chromatograph (Hewlett–Packard 5890 Series with autosampler) using an HP5 capillary column (30 m $\times$ 0.32 mm $\times$ 0.25 µm i.d.).

After the hydrogenation experiments the changes in platinum particle size of the spent catalysts were investigated with TEM. For PtCNF to PtCNF973 no significant modification in size and shape of the platinum particles was observed. The platinum particles in PtCNFnp, however, had sintered to 2–10 nm during the reaction under the rather severe conditions (4.8 MPa H_2 and 383 K).

To investigate whether the catalysts became irreversibly deactivated, three consecutive experiments with one catalyst batch of PtCNF were executed. Between the runs the catalyst was washed repeatedly with isopropanol and dried. The activity of the catalysts in the three runs was comparable, thus proving the absence of irreversible deactivation.

Duplicate experiments were performed with both PtCNF and PtCNF973 showing rates and selectivities to the various products to be within an error margin of around 5%, indicating excellent reproducibility.

Table 2
Number of oxygen atoms/nm^2 on CNF surface as a function of treatment temperature determined with acid–base titration, XPS, and TGA-MS

Sample	Titration		XPS		TGA-MS	
	Number of acid site/nm^2	O atoms/ nm^2	O/C atomic ratio	O atoms/ nm^2	Weight loss (%)	O atoms/ nm^2
CNFox	1.4 ± 0.1	2.8 ± 0.2	0.069	9.6 ± 1.4	5.7	9.8 ± 0.8
CNFox, 573 K in N$_2$	1.0 ± 0.1	2.0 ± 0.2	0.038	5.3 ± 0.8	3.7	6.3 ± 0.5
CNFox, 773 K in N$_2$	0.2 ± 0.02	0.4 ± 0.04	0.032	4.4 ± 0.7	3.3	5.6 ± 0.5
CNFox, 973 K in N$_2$	$\sim 0.03 \pm 0.003$	0.06 ± 0.01	0.017	2.3 ± 0.3	1.8	3.0 ± 0.3
PtCNFnp			0.044	6.1 ± 0.9	5.1	7.7 ± 0.6
PtCNF			0.038	5.3 ± 0.8	3.8	6.5 ± 0.5
PtCNF573			0.037	5.1 ± 0.8	3.7	6.2 ± 0.5
PtCNF773			0.026	3.6 ± 0.5	2.7	4.5 ± 0.5
PtCNF973			0.016	2.2 ± 0.3	1.5	2.6 ± 0.3

3. Results and discussion

3.1. Characterization of the CNF support

The CNF are of the fishbone type, i.e., with the graphite planes oriented at an angle to the central axis and the fibers interwoven into porous bodies. After removal of the growth catalyst and the activation treatment with nitric acid for 2 h the nonmicroporous fibers exhibited a specific surface area of 177 m^2/g. X-ray diffraction and TEM images demonstrated that the graphite-like structure of the CNF had not been affected during activation. From SEM and TEM micrographs an average fiber diameter of 25 nm could be derived with a narrow diameter distribution.

As stated earlier the activation procedure in nitric acid is carried out to introduce various types of oxygen functional groups on the CNF and to remove nonencapsulated nickel from the growth catalyst. TEM images show that the remaining nickel ($\leqslant 0.5$ wt%, XRF analysis) is encapsulated by graphitic envelopes, thus preventing interference in catalysis.

Table 2 lists the number of acid sites (p$K_a < 7.5$) of oxidized CNF treated at different temperatures in N$_2$ as determined by titration, as well as the number of oxygen atoms/nm^2 calculated from XPS and TGA-MS results. After activation and drying of the CNF 1.4 acid sites/nm^2 were present. Heat treatment resulted in a gradual removal of the majority of the acidic oxygen-containing groups to 0.03 acid sites/nm^2 after treatment at 973 K. XPS measurements were done to establish the amount of oxygen in the outer layer of 2–3 nm of the CNF. After oxidation and drying an O/C atomic ratio of 0.069 was found. A gradual decrease in the O/C ratio from 0.069 to 0.017 with increasing heat-treatment temperature was observed. Using a model the O/C ratios can be converted into a number of oxygen atoms/nm^2 [29]. These results (Table 2) show that fibers oxidized in HNO$_3$ for 2 h contain 9.6 O atoms/nm^2. Since oxygen-containing surface groups often contain one or two oxygen atoms, this implies that about 5–10 oxygen-containing surface groups would be present when it is assumed that all oxygen is located at the outer surface. Values up to 1–3 groups/nm^2, as earlier proposed by Boehm and as we found by titration, seem to be more realistic [30]. An explanation for this discrepancy can be found in the assumption that oxygen atoms are not exclusively present at the surface, but also are built in the subsurface (2–3 nm) graphene sheets [31,32]. TGA-MS up to 1123 K was used to establish the number of thermally removable oxygen atoms from the surface and the bulk of the CNF. Also TGA-MS results show the presence of oxygen-containing groups in the oxidized CNF and the partial removal of these groups with increasing heat treatment. The number of oxygen atoms as determined using XPS and TGA-MS is comparable when the error margins are taken into account. From these results it is concluded that oxygen is not present throughout the carbon support, but is mainly located in the outer 2–3 nm of the fibers with 2–30% present in acidic groups at the exterior surface, i.e., accessible for titration. It is noted that with increasing treatment temperature the ratio of (acidic oxygen at exterior)/(total oxygen) drops largely. For a more detailed investigation on the effect of oxidation and subsequent thermal treatment of CNF we refer to [23].

3.2. Characterization of the CNF-supported platinum catalysts

The metal loading of the Pt/CNF catalysts as established with XRF was 3.6 wt% (Table 1). TPR results (not shown) of the freshly loaded sample demonstrated that all catalysts were completely reduced at 473 K. Therefore all catalysts were reduced at this temperature. PtCNFnp was only reduced in situ at 383 K preceding the catalytic experiments, to maintain a support oxygen concentration as large as possible.

The amount of support oxygen still present on the platinum catalysts after the different treatments is assessed using XPS and TGA-MS (Table 2). Unfortunately, titration experiments could not be performed, since the presence of platinum interfered with the measurements. This table shows that due to the application of platinum on the CNF the average number of oxygen atoms/nm^2 has decreased from about 9.7 (CNFox) to about 6.9 (PtCNFnp). A more detailed inves-
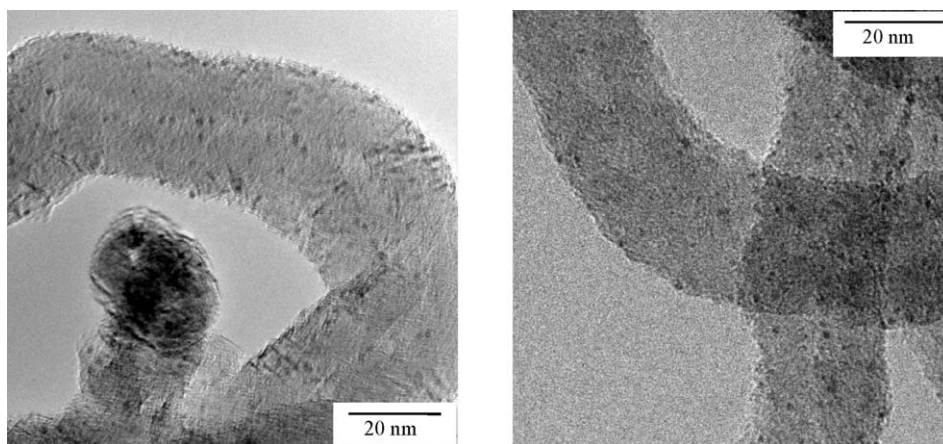
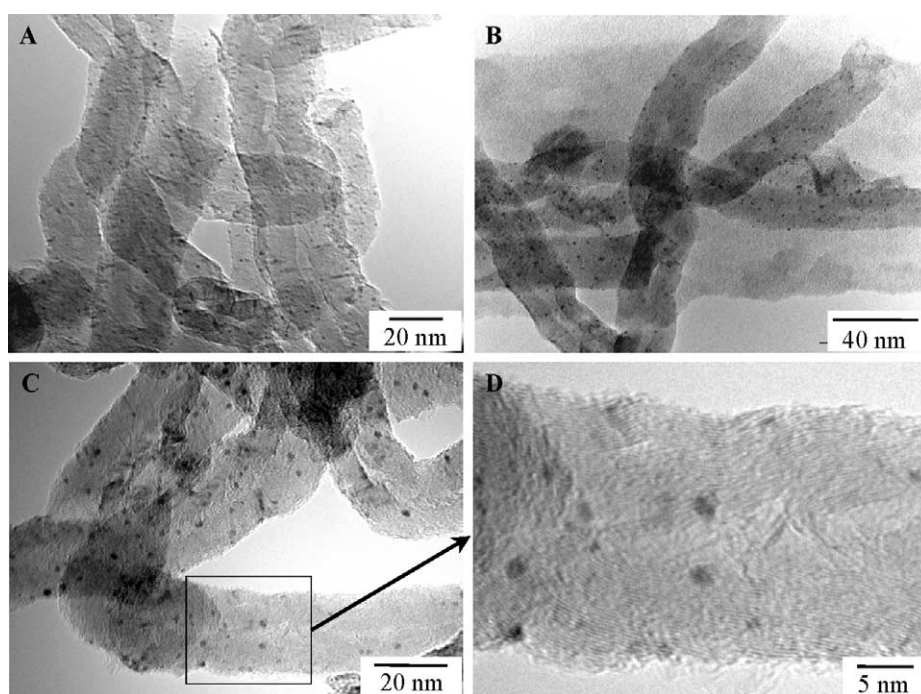Fig. 1. TEM images of CNF-supported platinum catalysts after reduction (PtCNF).

Fig. 2. TEM images of CNF-supported platinum catalysts after reduction and heat treatment in N_2 (A) PtCNF573, (B) PtCNF773, and (C and D) PtCNF973.

tigation on the relation between the oxygen groups and the metal loading can be found elsewhere [33]. Subsequent reduction and heat treatments resulted in a further gradual decrease in the amount of support oxygen to ultimately around 2–3 oxygen atoms/nm^2 for PtCNF973, very similar to the values observed with unloaded CNF.

In Fig. 1 two representative TEM images of PtCNF are shown. The platinum particles are small and homogeneously distributed over the CNF surface. The particle-size distribution is very narrow; particles of 1–2 nm are observed. The average particle size and H/Pt ratio calculated from hydrogen-chemisorption data are presented in Table 3. Using the total amount of adsorbed hydrogen a H/Pt of 0.79 an average platinum particle size of 1.4 nm was calculated for PtCNF.

Table 3
TEM and hydrogen chemisorption results at 308 K on the different CNF-supported platinum catalysts

Sample	TEM d (nm)	H$_2$ chemisorption				
		Irreversible		Total		H_{irr}/H_{tot}
		H/Pt	d (nm)	H/Pt	d (nm)	
PtCNF	1–2	0.37	3.1	0.79	1.4	0.45
PtCNF573	1–2	0.63	1.8	1.06	1.1	0.60
PtCNF773	1–2	0.33	3.5	0.74	1.5	0.42
PtCNF973	1–3	0.21	5.4	0.49	2.3	0.43

After reduction the platinum catalysts were treated in N_2 at 573, 773, and 973 K to remove part of the support oxygen-containing groups. From the TEM images (Figs. 2A–2D) it is clear that treatment at 573 and 773 K did not affect the platinum particle size, while treatment at 973 K resulted in a
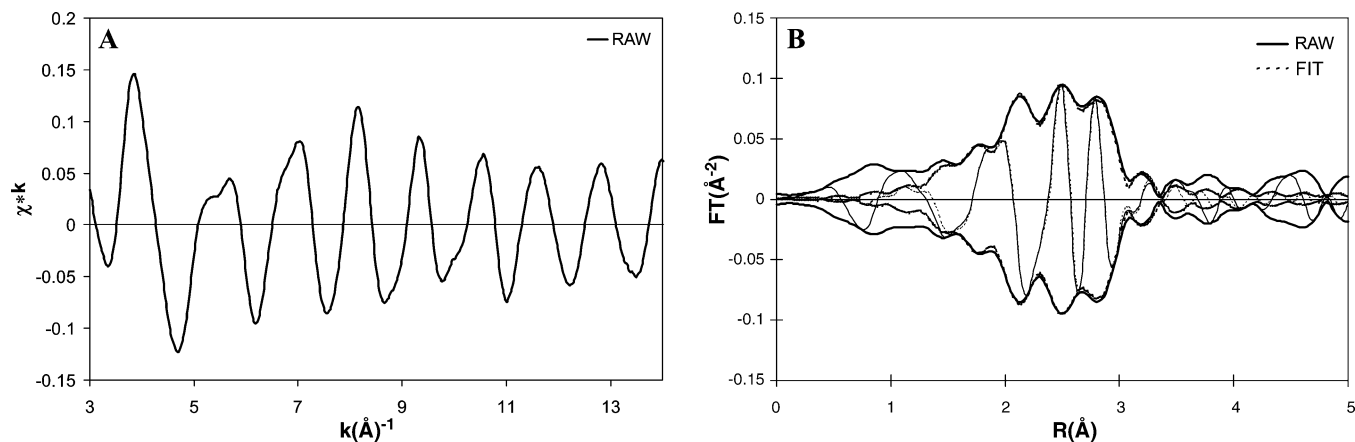
Fig. 3. (A) The EXAFS raw data (k^1 weighted, $\Delta k = 3$–14 Å) of PtCNF (RED). (B) The corresponding Fourier transforms (k^1 weighted, $\Delta k = 3$–14 Å) of the EXAFS raw data (solid line) and the total fit (dotted line).

small increase in particle size. In Fig. 2D the graphene sheets of the fishbone CNF covered with some platinum particles are visible. Hydrogen-chemisorption results (Table 3) show an unexpected and up to now unexplained increase in H/Pt from 0.79 for PtCNF to 1.06 for PtCNF573. After treatment at 773 and 973 K H/Pt ratios of 0.74 and 0.49 were found, indicating average particle sizes of 1.5 and 2.3 nm, respectively, thereby confirming TEM results.

EXAFS was used as an additional method to determine the structural parameters of the platinum particles in PtCNF and PtCNF773. Fig. 3A shows the experimental EXAFS data (k^1 weighted, $\Delta k = 3$–14 Å^{-1}) of PtCNF (RED) in a hydrogen atmosphere. The signal to noise ratio at $k = 4.4$ Å^{-1} amounts to approximately 150 on both the PtCNF and the PtCNF773 spectra, showing the data to have an excellent quality.

The corresponding k^1 Fourier transform of the raw EXAFS data of PtCNF (RED) is displayed in Fig. 3B. This is a typical example of the Fourier transform of small supported platinum particles using k^1 weighting. It contains both Pt–Pt and Pt–C(O) contributions. In this study, the separation of Pt–C and Pt–O contributions is not carried out, because it is difficult to identify O and C as different backscatterers since they are neighboring elements in the Periodic Table. The sum of Pt–C and Pt–O contributions is denoted as Pt–C(O). The parameters used to fit the experimental EXAFS data of PtCNF (RED) and PtCNF773 (RED) are given in Table 4. As an example Fig. 3B enables the comparison of the Fourier transforms of the raw EXAFS data (solid line) and the fit (dotted line) of PtCNF (RED) using the parameters listed in Table 4. This comparison demonstrates the excellent fit quality of all the EXAFS data. The C(O) and Pt backscatterers were identified using the difference file technique. The variances in imaginary and absolute parts were used to determine the fit quality. Fits with variances below 1% have been considered to represent good models for the experimental data.

The EXAFS results in Table 4 show a Pt–Pt bond distance in PtCNF and PtCNF773 of 2.77 and 2.76 Å, respec-

Table 4
Fit parameters of EXAFS spectra (Δk, 3–14 Å^{-1}; ΔR, 1.6–3.2 Å) and variances for model spectra of PtCNF (RED) and PtCNF773 (RED)

Catalyst (treatment)	Scatter	N ±10%	R (Å) ±0.02 Å	$\Delta\sigma^2$ (Å^2) ±5%	ΔE_0 (eV)	k^1 variance (%)	
					±10%	Im.	Abs.
PtCNF (RED)	C(O)$_s$	0.7	2.02	2.0×10^{-3}	1.2	0.39	0.14
	C(O)$_l$	1.6	2.65	2.2×10^{-3}	−0.3		
	Pt	5.2	2.77	1.1×10^{-3}	2.1		
PtCNF773 (RED)	C(O)$_s$	0.3	2.01	1.3×10^{-3}	3.2	0.34	0.12
	C(O)$_l$	2.0	2.62	1.4×10^{-3}	1.5		
	Pt	5.5	2.76	1.6×10^{-3}	1.3		

tively, which is typical for metallic platinum particles in a hydrogen atmosphere [34]. The Pt–Pt coordination numbers found are 5.2 (PtCNF) and 5.5 (PtCNF773). This shows that in both samples very small Pt particles with an average size of around 1 nm are present [35,36]. The other parameters of PtCNF and PtCNF773 differ only slightly or not at all. A full EXAFS study dealing with the structure of the metal–support interface in the Pt/CNF catalysts, the shortening of the Pt–C distance upon evacuation, and the role of oxygen-containing groups in stabilizing the platinum particles is published in a separate paper [37].

3.3. Hydrogenation of cinnamaldehyde

The hydrogenation of cinnamaldehyde can be presented by a simplified reaction pathway as shown in Fig. 4. In this study the main by-products before complete conversion of cinnamaldehyde were cinnamyl isopropylether and the di-isopropylacetal of hydrocinnamaldehyde. These products form via a reaction between cinnamaldehyde or hydrocinnamaldehyde and the solvent isopropanol.

For PtCNF and PtCNF973 Fig. 5 shows, as a function of time, the molar composition of the reaction mixture for cinnamaldehyde (CALD), the primary reaction products hydrocinnamaldehyde (HALD) and cinnamyl alcohol (CALC),
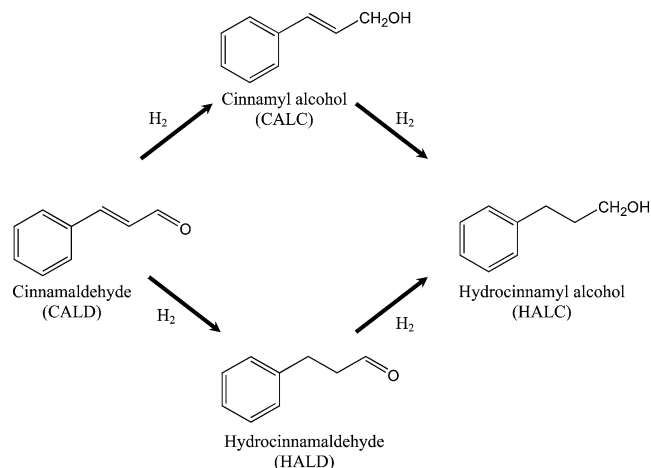
Fig. 4. Reaction pathway of the hydrogenation of cinnamaldehyde.

pletely converted within 20 min. The difference in activity will be dealt with in more detail below.

It is clear that the selectivities [selectivity $Y(\%) = (\text{moles } Y(t)/\text{moles CALD}(0)) \times 100\%$] to the main products are dependent on the catalyst. PtCNF produces cinnamyl alcohol and hydrocinnamaldehyde in comparable amounts. On the other hand, with PtCNF973 hydrocinnamaldehyde is the main product. In Fig. 6 the selectivities to cinnamyl alcohol (CALC) and hydrocinnamaldehyde (HALD) are plotted as a function of the conversion [conversion $(\%) = (1 - (\text{moles CALD}(t)/\text{moles CALD}(0))) \times 100\%$] and in Table 5 the selectivities at 60% conversion to the various reaction products and the two main byproducts are represented. For PtCNFnp $S_{\text{CALC}} = 58\%$ and $S_{\text{HALD}} = 22\%$ is found. With increasing treatment temperature the selectivity toward the alcohol gradually declines and the selectivity to hydrocinnamaldehyde rises. For PtCNF973 $S_{\text{CALC}} = 8\%$, while $S_{\text{HALD}} = 74\%$. Obviously the rate of C=C hydrogenation of cinnamaldehyde is strongly enhanced with heat treatment of the catalyst, while the rate of hydrogenation of the C=O has only slightly increased. Fig. 5 demonstrates, however, that the secondary hydrogenation of hydrocinnamaldehyde

and the secondary product hydrocinnamyl alcohol (HALC). First of all, from these graphs the large difference in hydrogenation activity between PtCNF and PtCNF973 is striking. Using PtCNF after 600 min only 80% conversion is obtained, while using PtCNF973 cinnamaldehyde is com-
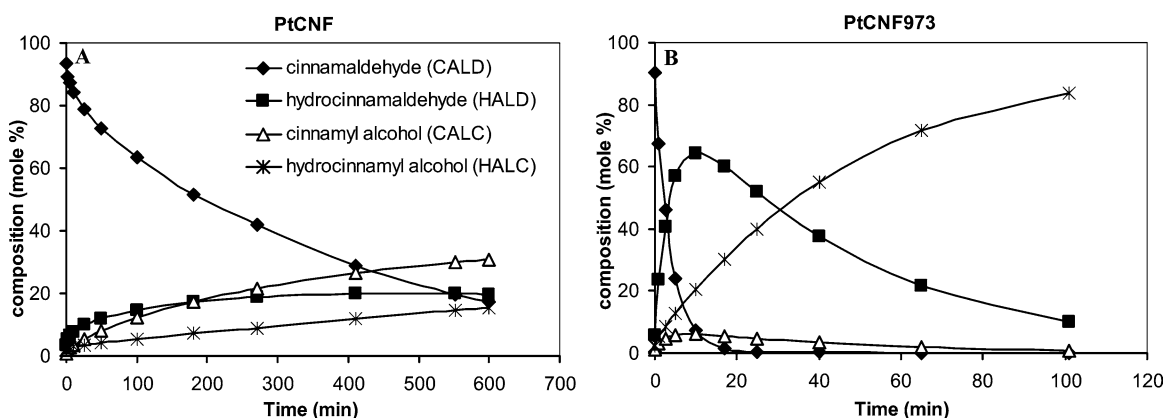

Fig. 5. Cinnamaldehyde conversion and product distribution as function of time on stream obtained at 383 K and 4.8 MPa hydrogen over CNF-supported platinum catalysts (A) PtCNF and (B) PtCNF973.
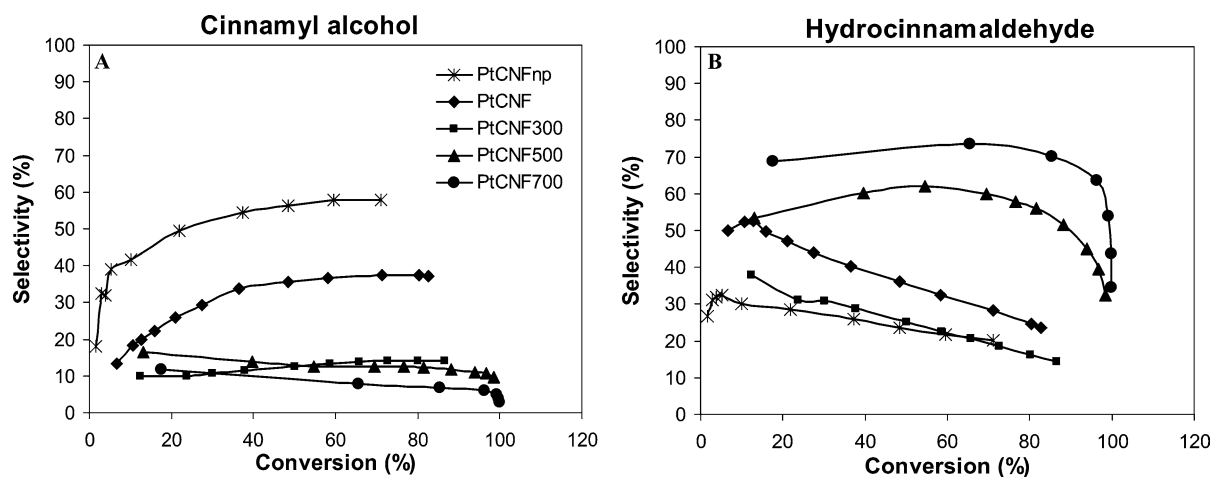

Fig. 6. Selectivities of different CNF-supported Pt catalysts as a function of conversion to (A) cinnamyl alcohol and (B) hydrocinnamaldehyde.

Table 5
Selectivity to cinnamyl alcohol, hydrocinnamaldehyde, hydrocinnamyl alcohol, and two by-products for cinnamaldehyde hydrogenation with CNF-supported platinum catalysts determined at 60% conversion

Sample name	S_{CALC} (mol%)	S_{HALD} (mol%)	S_{HALC} (mol%)	By-products	
				Cinnamyl isopropyl-ether	Di-isopropylace-tal of hydrocin-namaldehyde
PtCNFnp	58	22	13	1	1
PtCNF	37	32	15	2	6
PtCNF573	13	23	12	11	19
PtCNF773	13	61	17	1	2
PtCNF973	8	74	18	0	0

Table 6
Initial activities, relative activities, and TOF for cinnamaldehyde hydrogenation with CNF-supported platinum catalysts at 383 K and a hydrogen pressure of 4.8 MPa

Sample name	Initial activity (mmol/(min g_{cat}))	Relative activity[b]	TOF[a] (s^{-1})
PtCNFnp	0.60	1.0	n.d.[c]
PtCNF	1.9	3.2	0.23
PtCNF573	4.0	6.7	0.39
PtCNF773	11	19	1.6
PtCNF973	15	25	3.3

[a] Results are given in mole CALD hydrogenated per mole of platinum surface atoms in the catalyst per second. The amount of platinum surface atoms is calculated from the catalyst weight, the metal loading, and the H/Pt (total H) ratio.

[b] Relative activity is the initial activity divided by the initial activity of PtCNFnp.

[c] n.d., not determined because the H/Pt ratio is not known for this sample.

Table 7
Platinum $4f_{7/2}$ and $4f_{5/2}$ binding energies of the CNF-supported platinum catalysts after reduction at 383 K determined by XPS using Gauss–Lorenzian peak fits

Sample name	E_b (eV)	
	Pt $4f_{7/2}$	Pt $4f_{5/2}$
PtCNFnp	73.4	76.2
PtCNF	71.4	74.6
PtCNF573	71.4	74.7
PtCNF773	71.4	74.7
PtCNF973	71.6	74.6

to hydrocinnamyl alcohol is also much faster on PtCNF973; i.e., the C=O hydrogenation rate seems dependent on the substrate molecule.

Fig. 6 shows that the selectivities to the primary and secondary products depend on the conversion of cinnamaldehyde. Beyond 5% conversion the selectivity of the heat-treated catalysts remains fairly constant. Another striking feature is the strong dependence of the amount of formed by-products with the treatment of the catalyst (Table 5): PtCNFnp, PtCNF773, and PtCNF973 produce only minor amounts of the isopropanol ether and acetal, while PtCNF (2 and 6%) and especially PtCNF573 (11 and 19%) form large amounts of these products. It is well known that these type of reactions are acid-catalyzed [38]. Therefore, it is expected that with increasing heat treatment of the catalyst and thus with decreasing support acidity the amount of by-products drops. However, the low amount of by-products formed using PtCNFnp is unexpected.

Although the data show many interesting phenomena, in this paper we mainly focus on the effect of the oxygen-containing groups on the strongly enhanced activity for C=C hydrogenation in cinnamaldehyde. From the decrease in the concentration of cinnamaldehyde with time (Fig. 5) initial activities were calculated for all samples. These values are given in Table 6 together with the relative activity compared to the activity of PtCNFnp and the related TOF. Both Fig. 5 and Table 6 show the clear differences in catalytic behavior as a function of treatment temperature of the catalysts. With increasing treatment temperature a strong increase in the total activity was found. The observed activity of PtCNF973 was almost 25 times larger than that of PtCNFnp and almost 8 times larger than that of PtCNF. The TOFs differ even somewhat more due to a small increase in mean particle size in PtCNF973. This increase in total activity is mainly caused by a large increase in hydrocinnamaldehyde formation as can be concluded from Fig. 5.

Calculations of the Weisz–Prater criterion of PtCNF and PtCNF973 and calculated concentration profiles in the catalyst particles of these catalysts using a kinetic model, which includes mass transfer inside the catalyst particles, demonstrate that with PtCNF internal diffusion limitations are not apparent. In contrast, with PtCNF973 the increase in activity is such that diffusion of the organic compounds in the catalyst bodies limits the reaction rate [39]. From the latter calculation the ratio of the intrinsic activity of PtCNF and PtCNF973 is much larger than the factor of 8 in observed activitie.

3.4. Electronic structure of platinum

The hydrogenation results presented here using the Pt/CNF catalysts and the results reported in an earlier study on RuCNF catalysts [15] show that the catalytic behavior of CNF-supported noble metals is strongly dependent on the heat treatment and thus on the amount of oxygen groups present in/at the support surface. In order to investigate whether the oxygen-containing groups influence the electronic properties of the platinum particles, we executed XPS and H_2-chemisorption measurements. Using XPS a shift in platinum binding energy is expected [21,40] and with hydrogen chemisorption the H_{strong}/H_{total} ratio should change if a large electronic effect of the support is effective [41].

In Table 7 the platinum $4f_{7/2}$ and $4f_{5/2}$ binding energies are displayed as determined for the CNF-supported platinum catalysts after reduction using Gauss–Lorenzian peak fits. For metallic platinum, binding energies of 70.9 ($4f_{7/2}$) and
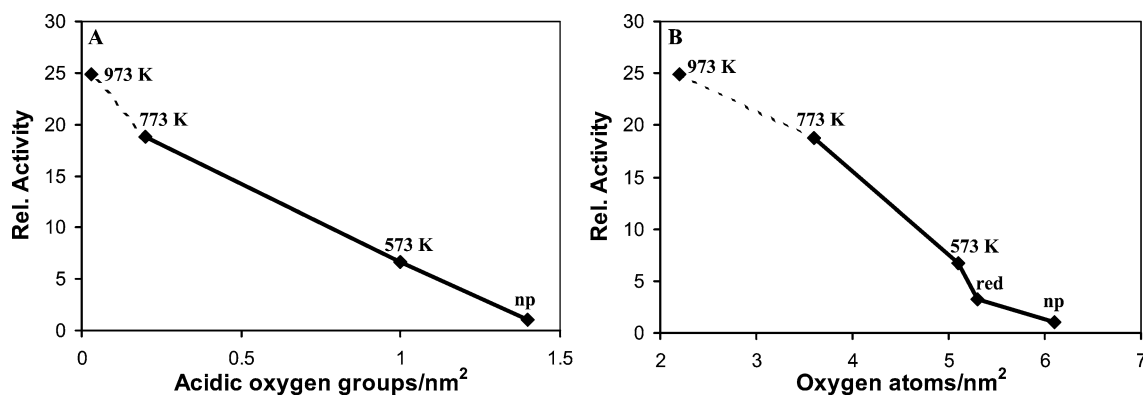
Fig. 7. Relative total activity for cinnamaldehyde hydrogenation as a function of the amount of acidic groups (A) and as a function of the amount of oxygen (XPS) on the CNF-supported platinum catalysts (B).

74.3 eV ($4f_{5/2}$) have been reported [42]. The results show that in PtCNF, PtCNF573, PtCNF773, and PtCNF973 the platinum binding energy is equal for all samples and around 71.4 and 74.6 eV, respectively, indicating that there is a shift of 0.3–0.5 eV compared to the binding energies of bulk platinum, probably due to the size of the metallic particles. The binding energy of PtCNFnp is slightly shifted to higher values, as ionic Pt species are present because of the mild reduction conditions.

With oxidic supports change of the electron richness of the support oxygen atoms was found to influence the metal binding energies of noble metal particles, i.e., higher binding energies when applied on supports with a relatively low oxygen electron density. Mojet et al., for instance, found a shift in binding energies of about 1.4 eV for both Pd $3d_{3/2}$ and Pd $3d_{5/3}$ in a Pd/LTL with a K/Al atomic ratio ranging from 0.55 to 1.10 [40]. Our results, however, indicate that the varying concentrations of oxygen groups on the carbon support do not give rise to these large shifts in platinum binding energies as determined with XPS.

In Table 3 the H_{irr}/H_{total} ratios of the various Pt/CNF catalysts are given. Oudenhuijzen [41] observed that for small LTL-supported platinum particles the hydrogen coverage and platinum–hydrogen binding strength depend on the support properties. For the various Pt/CNF catalysts no clear trend can be observed in the H_{strong}/H_{total} ratios.

Since we did not observe changes in the platinum binding energy and H_2 chemisorption we think that changes in electron density of the CNF support by partly removing the oxygen groups are much smaller than the changes in the electron density in oxidic-supported catalysts with, for example, varying K/Al ratios. These small changes in electronic properties are not revealed with XPS and H_2 chemisorption. However, in the accompanying paper differences are apparent in the order in hydrogen for the hydrogenation of cinnamaldehyde. Therefore, minor changes in the electronic properties of the platinum particles that are still important for catalysis cannot be excluded.

3.5. Oxygen content of the support

In Fig. 7A the relative total activity is plotted versus the amount of acidic oxygen-containing groups/nm^2 of the various CNF supports. Because titrimetric determination of the acidic groups on the Pt/CNF catalysts could not be effectuated due to the interfering action of platinum, we used the values found with the unloaded CNF support (see Table 2). An almost linear relation, especially for the PtCNFnp to PtCNF773 catalysts, is observed between the total activities and the concentration of acidic oxygen groups of the support. When only few acidic groups are present the activity is high and with increasing surface acidity the activities drop. The line between PtCNF773 and PtCNF973 is dotted, since the activity measured using PtCNF973 is influenced by internal diffusion limitation. Besides the acidic groups also other oxygen-containing surface groups are present on the CNF surface. Therefore, in Fig. 7B the relative total activities are plotted versus the number of oxygen atoms. For the number of oxygen atoms the values found with XPS are used. The correlation between activity and oxygen concentration is not as clear as between the activity and the number of acidic support surface groups, since the number of the acidic oxygen-containing groups is not linearly proportional to the total amount of oxygen on/in the fibers. These curves suggest that catalysis is directly influenced by the acidic oxygen-containing groups at the exterior surface of the CNF support. The strong increase in activity could be brought about by the removal of these support surface groups. A model in which the hydrogenation is assisted by adsorption of the cinnamaldehyde on the CNF support after removal of the oxygen surface groups is suggested. A full kinetic analysis of a series of cinnamaldehyde hydrogenation experiments underpins the effects of substrate adsorption on the support on catalysis [39].

4. Conclusions

Well-defined carbon nanofiber-supported platinum catalysts were prepared with a narrow size distribution, and a

mean particle size of 1–2 nm, both features being prerequisites for performing studies on the electronic support effect. By treatment of carbon nanofibers in nitric acid and subsequent loading, reduction, and heat treatment under nitrogen atmosphere, the concentration of oxygen-containing groups on the carbon nanofiber surface was varied without a significant change in platinum particle size.

The activity and selectivity in the liquid-phase hydrogenation of cinnamaldehyde was found to be dependent on the amount of oxygen of the CNF support. The rate of cinnamaldehyde conversion was enhanced with a factor of 25 after removal of the oxygen groups. The differences in intrinsic activities are even much larger, since with the catalyst treated at high temperatures internal diffusion limits the reaction rate. This enhanced activity is mainly caused by a strong increase in the hydrogenation rate of the C=C bond, while only a slight increase in C=O bond hydrogenation is observed.

Using XPS and H_2 chemisorption up to now no evidence has been found that the amount of oxygen in the support influences to a large extent the electronic properties of the platinum particles. Apparently modification of the electronic properties of the metal is not the prime cause of the large changes in catalytic behavior of the catalysts. A linear correlation between the increasing observed hydrogenation activity and the decreasing number of acidic groups on the carbon nanofiber support was found. Therefore, a model in which the hydrogenation is assisted by adsorption of the cinnamaldehyde on the CNF support after removal of the oxygen surface groups is suggested.

Acknowledgments

References

[1] P. Kluson, L. Cerveny, Appl. Catal. A 128 (1995) 13.

[2] V. Ponec, Appl. Catal. A 149 (1997) 27.

[3] B. Coq, F. Figueras, Coord. Chem. Rev. 178–180 (1998) 1753.

[4] P. Gallezot, D. Richard, Catal. Rev.-Sci. Eng. 40 (1998) 81.

[5] A. Giroir-Fendler, D. Richard, P. Gallezot, Stud. Surf. Sci. Catal. 41 (1988) 171.

[6] B. Coq, P.S. Kumbhar, C. Moreau, P. Moreau, M.G. Warawdekar, J. Mol. Catal. 85 (1993) 215.

[7] P.S. Kumbhar, B. Coq, C. Moreau, P. Moreau, J.M. Planeix, M.G. Warawdekar, in: N.M. Gupta, D.K. Chakrabarty (Eds.), Catalysis: Modern Trends, Narosa, New Delhi, 1995.

[8] A.B. da Silva, E. Jordoa, M.J. Mendes, P. Fouilloux, Appl. Catal. A 148 (1996) 253.

[9] C.M.G. van de Moesdijk and M.A.R. Bosma, US 4745234 (1988).

[10] P. Serp, M. Corrias, P. Kalck, Appl. Catal. A 253 (2003) 337.

[11] J.M. Planeix, N. Coustel, B. Coq, V. Brotons, P.S. Kumbhar, R. Dutartre, P. Geneste, P. Bernier, P.M. Ajayan, J. Am. Chem. Soc. 116 (1994) 7935.

[12] M. Lashdaf, A. Hase, E. Kauppinen, A.O.I. Krause, Catal. Lett. 52 (1998) 199.

[13] S. Galvagno, G. Capanelli, G. Neri, A. Donato, R. Pietropaolo, J. Mol. Catal. 64 (1991) 237.

[14] T. Vergunst, F. Kapteijn, J.A. Moulijn, Catal. Today 66 (2001) 381.

[15] M.L. Toebes, F.F. Prinsloo, J.H. Bitter, A.J. van Dillen, K.P. de Jong, J. Catal. 214 (2003) 78.

[16] R. Burch, A.R. Flambard, J. Catal. 78 (1982) 389.

[17] M. Haruta, S. Tsubota, T. Kobayashi, M.J. Genet, B. Delmon, J. Catal. 144 (1993) 175.

[18] J.H. Bitter, K. Seshan, J.A. Lercher, J. Catal. 171 (1997) 279.

[19] D.E. Ramaker, J. de Graaf, J.A.R. van Veen, D.C. Koningsberger, J. Catal. 203 (2001) 7.

[20] D.C. Koningsberger, M.K. Oudenhuijzen, J. de Graaf, J.A. van Bokhoven, D.E. Ramaker, J. Catal. 216 (2003) 178.

[21] B.L. Mojet, J.T. Miller, D.E. Ramaker, D.C. Koningsberger, J. Catal. 186 (1999) 373.

[22] A.Yu. Stakheev, L.M. Kustov, Appl. Catal. A 188 (1999) 3.

[23] M.L. Toebes, J.M.P. van Heeswijk, J.H. Bitter, A.J. van Dillen, K.P. de Jong, Carbon 42 (2004) 307.

[24] M.K. Oudenhuijzen, J.H. Bitter, D.C. Koningsberger, J. Phys. Chem. B 105 (2001) 4616.

[25] J.J.F. Scholten, A.P. Pijpers, A.M.L. Hustings, Catal. Rev.-Sci. Eng. 27 (1985) 151.

[26] M. Vaarkamp, J.C. Linders, D.C. Koningsberger, Phys. B 208–209 (1995) 159.

[27] D.C. Koningsberger, B.L. Mojet, G.E. van Dorssen, D.E. Ramaker, Top. Catal. 10 (2000) 143.

[28] D.C. Koningsberger, J. de Graaf, B.L. Mojet, D.E. Ramaker, J.T. Miller, Appl. Catal. A 191 (2000) 205.

[29] O.L.J. Gijzeman, unpublished results.

[30] H.P. Boehm, Adv. Catal. 16 (1966) 179.

[31] T.G. Ros, A.J. van Dillen, J.W. Geus, D.C. Koningsberger, Chem. Eur. J. 8 (2002) 1151.

[32] H. He, J. Klinowski, M. Fortser, A. Lerf, Chem. Phys. Lett. 287 (1998) 53.

[33] M.L. Toebes, L.M. Tang, M.H. Huis, van't Veld, J.H. Bitter, A.J. van Dillen, K.P. de Jong, J. Phys. Chem. B, in press.

[34] M.K. Oudenhuijzen, J.H. Bitter, D.C. Koningsberger, J. Phys. Chem. B 105 (2001) 4616.

[35] B.J. Kip, F.B.M. Duivenvoorden, D.C. Koningsberger, R. Prins, J. Catal. 105 (1987) 26.

[36] J. de Graaf, A.J. van Dillen, K.P. de Jong, D.C. Koningsberger, J. Catal. 203 (2001) 307.

[37] Y. Zhang, M.L. Toebes, W.E. O'Grady, A. van der Eerden, K.P. de Jong, D.C. Koningsberger, J. Phys. Chem. B, submitted.

[38] R.T. Morrison, R.N. Boyd, Organic Chemistry, Prentice-Hall, NJ, 1992.

[39] M.L. Toebes, T.A. Nijhuis, J. Hájek, J.H. Bitter, A.J. van Dillen, D.Y. Murzin, K.P. de Jong, part II, submitted.

[40] B.L. Mojet, M.J. Kappers, J.C. Muijsers, J.W. Niemantsverdriet, J.T. Miller, F.S. Modica, D.C. Koningsberger, Stud. Surf. Sci. Catal. 84 (1994) 909.

[41] M.K. Oudenhuijzen, Ph.D. thesis, Utrecht University, 2002.

[42] C.D. Wagner, W.M. Riggs, L.E. Davis, J.F. Moulder, G.E. Muilenberg (Eds.), Handbook of X-Ray Photoelectron Spectroscopy, Perkin–Elmer Corporation, Eden Prairie, MN, 1978.